Oxygen Defects Containing TiN Films for the Hydrogen Evolution Reaction: A Robust Thin Film Electrocatalyst With Outstanding Performance

Ayoub Laghrissi and Mohammed Es-Souni *

Posted Date: 29 March 2024

doi: 10.20944/preprints202403.1821.v1

Keywords: Hydrogen evolution reaction; Titanium nitride; Oxygen defects; TiNO; linear sweep voltammertry; DFT

Article

Oxygen Defects Containing TiN Films for the Hydrogen Evolution Reaction: A Robust Thin Film Electrocatalyst with Outstanding Performance

Ayoub Laghrissi [1] and Mohammed Es-Souni [2,*]

[1] Currently at Mads Clausen Institute, University of Southern Denmark, 6400 Sønderborg; laghrissi@mci.sdu.dk

[2] Institute of Materials and Surface Technology, Honorary Member of Kiel University of Applied Sciences, 24249 Kiel, Germany

* Correspondence: mohammed.es-souni@fh-kiel.de

Abstract: Density functional theory (DFT) calculations of hydrogen adsorption on titanium nitride had previously shown that hydrogen may adsorb on both titanium and nitrogen sites with a moderate adsorption energy. Further, the diffusion barrier was also found to be low. These findings may qualify TiN, a versatile multifunctional material with electronic conductivity, as electrode material for the hydrogen evolution reaction (HER). This was the main impetus of this work which aims to experimentally and theoretically investigate the electrocatalytic properties of TiN-layers that were processed on Ti substrate using reactive ion sputtering. The properties are discussed focusing on the role of oxygen defects introduced during the sputtering process on the HER. Based on DFT calculations, it is shown that these oxygen defects alter the electronic environment of the Ti atoms which entails a low hydrogen adsorption energy in the range of -0.1 eV; this leads to HER performances that match those of Pt-NPs in acidic media. When a few nanometr thick layer of Pd-NPs is sputtered on-top of the TiN-layer, the performance is drastically reduced. This is interpreted in terms of oxygen defects being scavenged by the Pd-NPs near the surface which is thought to reduce the hydrogen adsorption sites.

Keywords: hydrogen evolution reaction; titanium nitride; oxygen defects; TiNO; linear sweep voltammertry; DFT

1. Introduction

The share of renewables in the energy mix has seen a steep increase in the last decade, primarily driven by environmental concerns. In many regions of the world, the share of renewables is now at least 20% and is expected to increase during the coming decade to 40 or even 50% [1,2]. Recent developments in Li-ion battery modules that became much more competitive, as Li price on the world market continues to fall, have made it possible to efficiently store energy and release it to the grid in case of fluctuations in solar and wind power [3]; this certainly has contributed to widespread acceptability of renewables by commercial stakeholders. Nevertheless, an efficient exploitation of renewables will also have to consider other energy storage possibilities, such as (super)capacitors and water electrolysis, to mention only the electrochemical methods. In particular, water electrolysis, mainly for the production of green hydrogen via the hydrogen evolution reaction (HER), is highly attractive, and could afford a powerful way for energy storage that is clean and sustainable and could be used even in remote and desertic regions.

HER is a well-known electrochemical interfacial process that essentially depends on pH, catalyst, and applied voltage. The reaction mechanisms and kinetics involved at the interface between electrolyte and catalyst have been described in detail in numerous review articles, e.g., article by Conway and Tilak [4], Bockris and Conway [5], and Eley et al. [6], to mention only a few. The generally accepted reaction steps using a metal (M) catalyst under acidic conditions are [4–6]:

$$H_3O^+ + M + e^- \rightarrow MH_{ads} + H_2O \qquad \text{(Volmer step) (1)}$$

 doi:10.20944/preprints202403.1821.v1

followed by reactions (2) and/or (3)

$$H_3O^+ + M + e^- \rightarrow MH_{ads} + H_2O \quad \text{(Heyrovsky step)} \quad (2)$$

$$2MH_{ads} \rightarrow H_{2\uparrow} + 2M \quad \text{(Tafel step)} \quad (3)$$

Practically, the Tafel Equation (4) is used to evaluate catalyst's performance.

$$U_O = \beta log \frac{J}{J_0} \quad (4),$$

where U_O is the hydrogen overpotential, β and J_0 are temperature dependant materials constants, and J the measured current. $\beta = 2.3RT/\alpha F$ with R the gas constant, T the absolute temperature, F the Faraday constant, and α a constant. J_0 is the exchange current density representing the equilibrium exchange current density of the forward and reverse reactions at the electrode. From Equation (4) we may infer that the larger J_0 and α the smaller the overpotential U_O, a measure of a catalyst's performance.

The mechanisms of HER have been rationalized by different authors in terms of the rate-determining mechanisms (Equations (1) to (3)), considering the different acting kinetics parameters such as adsorbed hydrogen surface coverage, overpotential and pH (e.g., Conway and Tilak [4], Bhardwaj et al. [7], Shingawa et al. [8]). A critical parameter that has been largely discussed in the literature is the hydrogen adsorption energy, E_{C-H}, on the catalyst's (C) surface which governs the hydrogen surface coverage and the rate-limiting step of diffusion. Together with the exchange current density, i_0, from the Tafel equation, E_{C-H} has been used to evaluate catalysts via the so-called volcano plot [8–11]. In simple terms, one may state that a moderate E_{C-H} and a higher i_0 may constitute a meaningful materials selection criterium for catalysts development. To date, Pt has an unchallenged position at the top of the volcano, precisely because of the criteria mentioned above, and any new electrode material will be measured against the performance of Pt. However, Pt is a precious, strategic noble metal with limited resources, a fact that has triggered a spate of research for alternative materials. Several catalysts have been reported in the literature for the HER, including transition metals and various compounds, as compiled in the review article of Eftikhari [9]. Catalyst performance is generally weighed in terms of the magnitude of overpotential necessary for HER at a given pH, the current density generated/weight of the active catalyst and durability/stability. As mentioned above, Pt that is mostly used in acidic conditions is well known for its outstanding performance [12–15]. In particular, Pt-NPs are the best known HER catalysts to date, performing at very low overpotentials. Noble metal-free catalysts such as Ni and Ni-Mo [16], metal compounds, including FeS_2, MoS_2 [17], as well metalloids compounds such as C_3N_4 [18], to mention only a few of them, have been reported with acceptable performances, albeit stability issues have arisen. Also, while some of the catalysts mentioned above may perform well in tiny batches, their scalability is questionable as multiple processing steps are involved which complicates quality management and reproducibility of the results. New and efficient noble-metal-free HER catalysts that can be scaled-up using well established industrial processes are therefore of critical importance, as they will allow to cut electrode cost.

In the present work, the potential application of TiN as HER catalyst is considered. TiN is a well-established multifunctional material with applications spanning hard-coating for steel tools to plasmonics [19–21]; it is usually processed in industrial scale as thin film of various thickness using physical (PVD) or chemical (CVD) vapor deposition (e.g., review articles [22,23]). Further, it has been shown using density functional theory that hydrogen adsorbs on TiN with the adsorption energy being dependent on termination (N or Ti) and adsorption sites. [24,25] The values obtained on TiN (111) range from 0.60 to 3.11 eV for N-termination and from 1.93 to 3.59 eV for Ti termination [24]. A slightly different values were obtained by Siodmiak et al. on TiN (100) surface [25]. Overall, the adsorption energies are considered to be moderate, albeit larger than on Pt. The diffusion barrier along the crystal sites was also shown to be rather low. This would unveil a promising non-noble metal electrocatalyst electrodes that are chemically and mechanically resistant. More advantages lie in the well-documented fact that they can be processed on an industrial scale using versatile and commercially available industrial equipment. It will be shown in this paper that TiN thin films of approximately 400 nm, deposited on Ti substrates via reactive gas sputtering, are potent HER catalysts in acidic media with current densities in the range of -70 mA/cm^2 at an overpotential of -0.1

 doi:10.20944/preprints202403.1821.v1

V vs. SHE which is in the range of the performance of Pt/C. This performance is primarily ascribed to the existence of oxygen defects on the surface. It will also be indirectly shown that the TiN surface adsorption sites are critical for HER; few nanometres of sputtered Pd lead indeed to a drastic decrease in performance.

2. Materials and Methods

2.1. Synthesis and Characterization

Commercially pure, grade 1 Titanium sheets, 0.1 mm thick, were purchased in the annealed, oxide scale free and straightened condition from Goodfellow (Goodfellow, Germany). They were cut into 5x5 cm^2 samples, degreased in 99,9% ethanol in an ultrasonic bath, rinsed twice with ethanol and dried with compressed air, before introduction into the PVD chamber (PVD75, Lesker, Jefferson Hills, USA; electron beam system from Ferrotec GmbH, Unterensingen, Germany). An adhesion layer of 2 nm Ti was magnetron sputtered on the substrate surface using a Ti-target. On-top of the heterostructure above, the TiN layers were processed via reactive ion sputtering using 99.995 pure Titanium pellets (Lesker) and high-purity nitrogen (99.9999%, Westfalen AG, Germany). The following conditions were found to yield nearly stoichiometric TiN: electron beam evaporation of Ti at 8.75 kV and 65 to 90 mA in a mixture of nitrogen and Argon at a ratio of 8/15 and a pressure of 2 to $5x10^{-3}$ Torr. Under these conditions, the sputtering rate was in the range between 0.18 to 0.21 nm/s. The total sputtered thickness was 400 nm. The layer-thickness was cross-checked on cross-sections of coated Si that was introduced together with the Ti-substrates.

The microstructure and morphology of the samples were characterized with a high-resolution scanning electron microscope (SEM Ultra Plus, ZEISS, Oberkochen, Germany) operating in the secondary (SE) and energy selective backscattered (ESB) electron modes. The SEM is also equipped with an energy dispersive X-ray spectroscopy (EDS) package (INCAx-act, Oxford Instruments, High Wycombe, UK). The structure was characterized by X-ray diffraction (XRD, X'Pert Pro diffractometer PANalytical, Eindhoven, Netherland) in grazing incidence diffraction mode with constant $\theta = 1°$ using monochromatic CuKα radiation with $\lambda = 1.5418$ Å. The device has a full width to half maximum resolution of 0.03°.

An electrochemical workstation (ZAHNER IM6e, Kronach, Germany) was used for linear sweep voltammetry (LSV) measurements from -0.8 V to 0.3 V. The electrochemical experiments were performed in 0.5 M H_2SO_4 solution with pH 0.36, using a three-electrode set-up with a Pt mesh and HydroFlex (reversible H_2 reference electrode) as counter and reference electrodes, respectively. The ratio of the working electrode (WE) area to that the counter electrode (CE) was approximately 1 to 4. All potentials were referenced to the reversible hydrogen electrode (RHE). The current was normalized by the sample's measured area. All the H_2SO_4 solutions were saturated with Forming gas N_2+H_2 (after the usual bubbling with nitrogen) before measurement.

2.2. DFT Calculations

Using the Quantum ESPRESSO v.6.0 package [26–28], ab initio calculations based on density functional theory were conducted to calculate charge distribution and hydrogen adsorption on 111- and 100-oriented TiN surfaces. In the present study, electro-ion interactions were described using projector augmented wave (PAW) potentials, while exchange correlations were represented using generalized gradient approximations (GGA) based on Perdew-Burke-Ernzerhof (PBE) frameworks [29]. A 400 eV plane wave basis cut-off energy was set for the initial optimization of the structures by relaxing atomic positions using the Broyden-Fletcher-Goldfarb-Shanno (BFGS) method. To achieve high accuracy, a self-convergence field convergence criterion of 10-6 electrons was used. In Figure 1, hydrogen adsorption is shown in various locations, namely top N, top Ti, bridge for TiN (100), and topTi, topN, bridge, hollow for TiN (111). Oxygen defects were introduced by replacing nitrogen atoms with oxygen, following the formula $Ti_{(1-x/3)}Ti_{(vac)x}N_{1-x}O_x$, where x is set to 0.1. This specific concentration of oxygen ensures a calculated change in crystal structure that mainly affects the surface layer, while the bulk layers remain unchanged [30]. This selective modification aims to

 doi:10.20944/preprints202403.1821.v1

explore changes in surface properties, such as reactivity and electronic structure, without significantly altering the overall properties of the material. The introduction of oxygen to the surface layer of TiN (111) represents a focused approach to modify material properties for targeted applications. To achieve the most stable surface hydrogen distance, the hydrogen atom and the top layer of the plate were allowed to relax their atomic positions. To calculate the hydrogen adsorption energies, the the usual definition of Equation (5) is used:

$$Eads = E_{Metal-H} - (E_{metal} + {}^{1}/_{2}\, E_{H_2}) \quad (5)$$

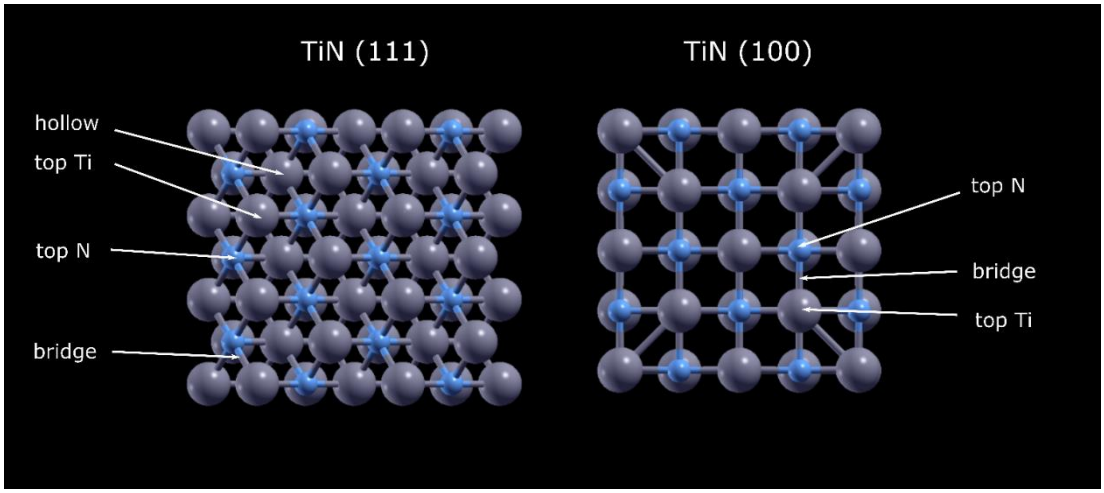

Figure 1. Top view of modeled TiN(100) and TiN(111) with possible adsorption sites.

3. Results

3.1. Morphology Structure and Chemistry

Large area, homogeneous TiN films are obtained on Ti-sheets using the experimental conditions depicted in the experimental section. A photograph of a 10x10 cm² sample is shown in Figure S1 (supplementary information). The morphology of the TiN layers is displayed in Figure 2. The top-view SEM micrographs, Figure 2a,b, show faceted star-like shaped nanocrystals that seem to build-up individually, independent from one another, and leading to a highly porous, rugged surface. This morphology may arise from the different growth velocities of differently oriented nanocrystals. Note that the pyramidal crystals (predominantly 111 orientation) top the surface (apparent from their brighter contrast in the secondary electron micrographs which arises from their higher vicinity to the in-lens detector). The cross-section micrograph of Figure 2c indeed shows that the poly-nanocrystals grow perpendicular to the interface from highly dense nucleation sites, conferring to them a columnar morphology. One might also see that the crystals are in many areas separated by voids. As will be shown below (see the XPS results), oxygen defects are present in the TiN-layer, probably incorporated during reactive sputtering owing to residual oxygen pressure in the chamber. As divalent oxygen ions are replacing trivalent nitrogen ions, Ti^{3+} vacancies are created to ensure electric neutrality (see below for discussion). The presence of these defects entails specific properties of $Ti(N,O)_x$ that are different from TiN or TiO_2, although the rock salt structure remains roughly unaltered [30]. To qualitatively assess the impact of the surface defects on HER, a thin Pd layer of approximately 10 nm was sputtered on top of the TiN layer in a second experiment, Figure 3. This should completely or partially saturate the $Ti(N,O)_x$ surface sites with Pd, a known HER catalyst.

 doi:10.20944/preprints202403.1821.v1

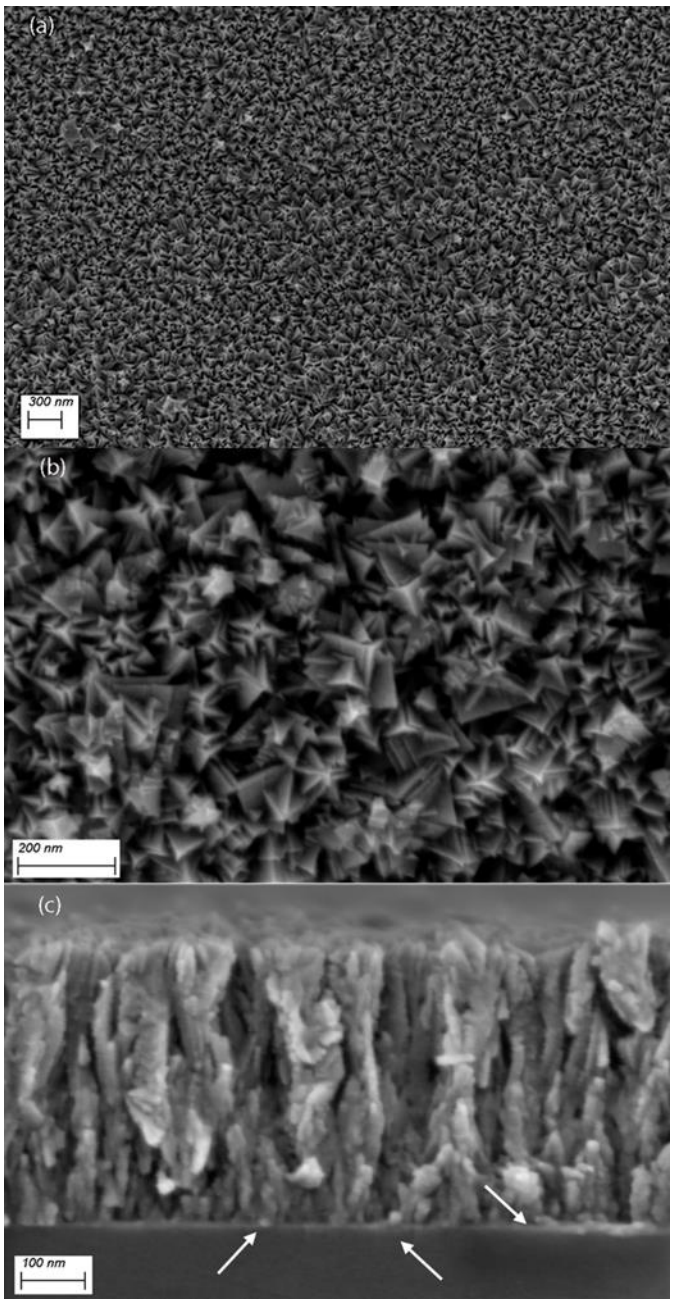

Figure 2. top-view secondary electron (SE) micrographs of the TiN layers on Ti-substrate (a) and (b) which show at two different magnifications the particular morphology of the poly-nanocrystals with their faceted and rugged appearance. (c) is a cross-section micrograph obtained on a silicon substrate that was coated under the same conditions. Notice the perpendicular growth from high density nucleation sites at the interface (arrows).

The XRD patterns are displayed in Figure 4. There are traces of The TiO_2-rutile phase on/in the Ti sheet which might originate from earlier processing. The reflexes pertaining to TiN could be assigned to the non-stoichiometric $TiN_{0.88}$ phase (PDF card no 01-087-0630) with predominance of the 111 orientation. Also, in this sample traces of rutile might be present, but are difficult to ascertain as the peaks are faint, and the most intense rutile reflexes (R110) could not be detected. The sample with Pd-NPs on top of the TiN-layer shows only one faint Pd reflex, but EDS analysis is conclusive about the presence of Pd, Figure 3e.

 doi:10.20944/preprints202403.1821.v1

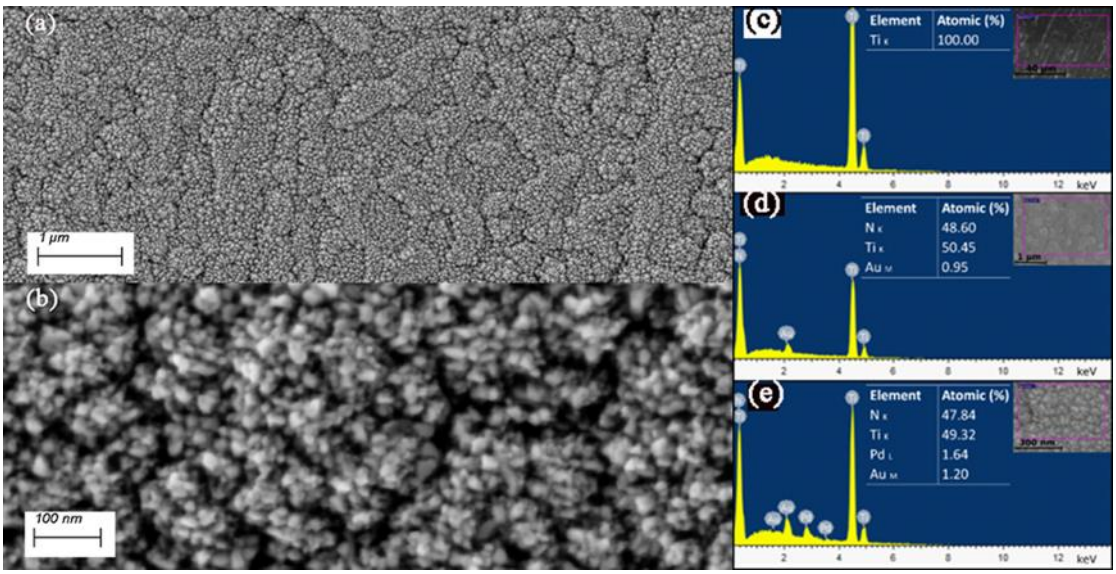

Figure 3. SE micrographs of the Ti-TiN-Pd -layer at low (a) and high magnification (b) which show Pd-NPs topping the TiN crystal spikes. The right images show EDS analysis of Ti (c), TiN (d) and Ti-TiN-Pd (e).

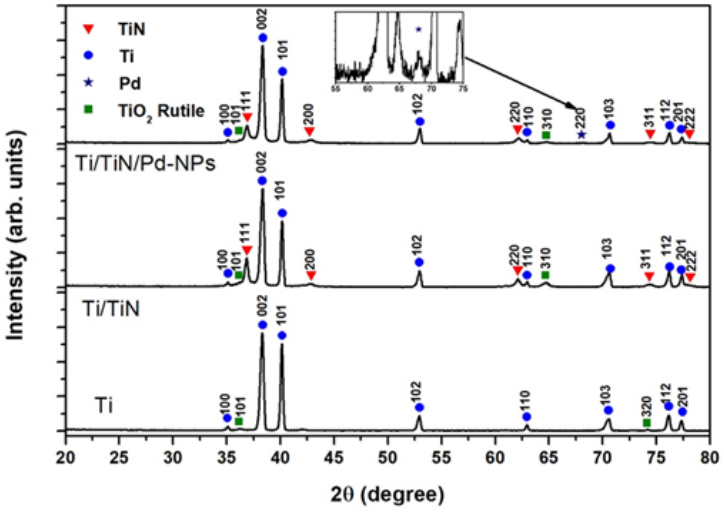

Figure 4. XRD patterns of the substrate Ti, Ti/TiN and the Ti/TiN-Pd composite layer. The TiN pattern is indexed according to the PDF card # 01-087-0630 for the non-stoichiometric phase $TiN_{0.88}$ (see below for discussion). The inset in the upper pattern is an enlargement of the pattern containing the 220 Pd reflex (*).

To investigate the surface chemistry of the TiN layer, X-ray photoelectron spectroscopy measurements were performed after argon ions cleaning. The high-resolution XPS peaks of Ti2p, N1s, O1s and C1s are displayed in Figure 5. The carbon 1s peak arises from surface contamination and cannot be associated with any compound at the surface. The doublet $Ti2p_{1/2}$ and $Ti2p_{3/2}$ of the Ti2p peak shows energy levels that can be attributed to Ti-O in TiO_2 and Ti-N in TiN bonds. Together with the binding energies of N1s and O1s, and owing to XPS being sensitive to surface chemistry, the formation of a TiN_xO_{1-x} (TiNO) layer at the surface, reported in previous work [30–33] can be ascertained. Notwithstanding this fact, oxygen defects probably are present in the TiN_x bulk as well, not least because in the processing method used oxygen cannot be wholly eliminated from the chamber, leaving sufficient oxygen partial pressure for the formation of the defects observed.

 doi:10.20944/preprints202403.1821.v1

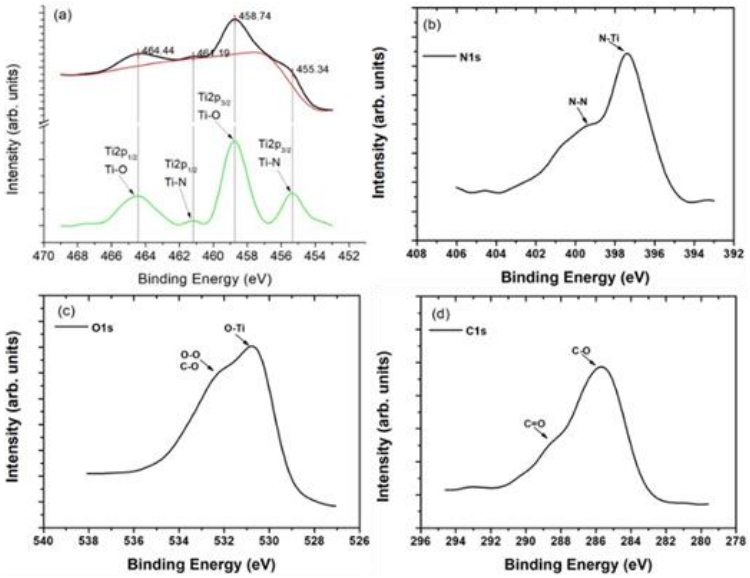

Figure 5. XPS of Ti/TiN showing the core levels of Ti2p, N1s, O1s and C1s (see main text for more details). The measured Ti2p in (a) is deconvoluted in the green curve, showing bonding energies of the different compounds.

3.2. HER Investigations

The linear sweep voltammetry (LSV) curves are shown in Figure 6a for the plain Ti-substrate, Ti/TiNO and Ti/TiNO-PdNPs. There is undeniably a huge difference in the HER behavior, depending on the sample chemistry. While the Ti-substrate rather shows a flat LSV curve with faint activity (Ti is known for its activity for the HER at high overpotentials) [34], a drastic increase in the current density is observed with the TiNO layer which shows an almost two orders of magnitude higher values (in comparison to Ti, e.g., at -0.1V). The overpotential for the HER is also drastically reduced and rivals the values reported for the best-known C/Pt-NPs catalysts [35]. This activity is also higher than what is reported in literature for TiN nanowires (NW) in 1M $HClO_4$ [36]. When a thin Pd layer is sputtered on TiNO, there is a conspicuous decrease in the current density and an increase in the overpotential, in comparison to pristine TiNO (e.g., approximately -2 mA/cm^2 in comparison to -40 mA/cm^2 for Ti-TiNO at an overpotential of -0.05 V), Figure 6a. Considering the EIS spectra, Figure 6c-d, it is readily seen that for both electrodes the data are well described by an almost perfect half-circle (apart from the data pertaining to the -0.1 V overpotential, Figure 6c, where an additional process is probably operating) suggesting a reactive system consisting of a series resistance, R_s (the ohmic resistance of the electrolyte) and a charge transfer resistance, R_{ct}, in parallel with a capacitance element [37].

 doi:10.20944/preprints202403.1821.v1

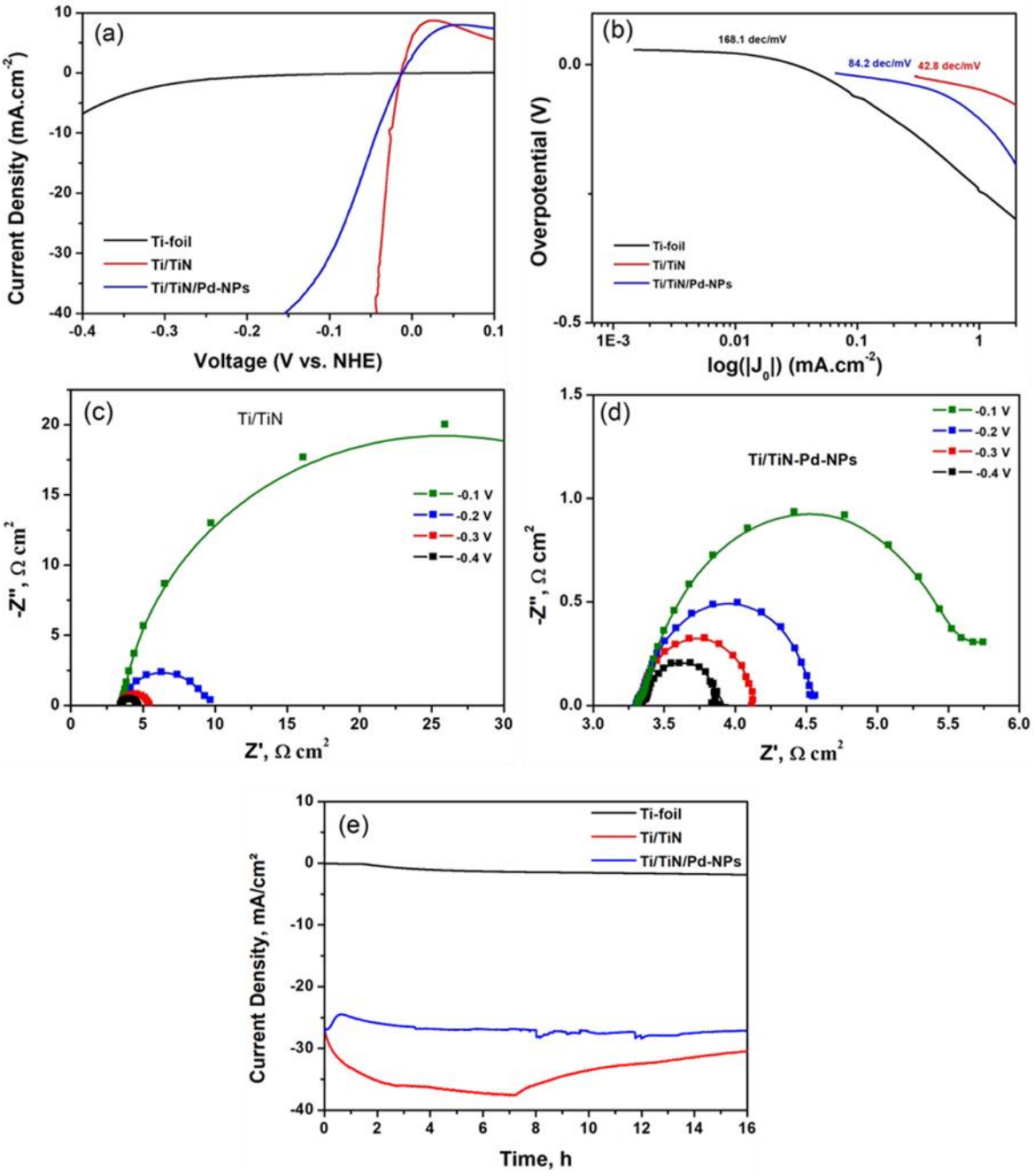

Figure 6. (a) IR-corrected linear sweep voltammograms in 0.5 M H_2SO_4 of TiNO and TiNO-PdNPs. (b) Tafel plots corresponding to the LSV curves. The current density is normalised by the geometric surface area. Electrochemical impedance spectroscopy at different over potentials of -0.1, -0.2, -0.3 and -0.4 V for (c) TiNO and (d) TiNO-PdNPs. (e) Chronoamperometric curves in 0.5 M H_2SO_4 at -0.4 V for 16 hours.

The data unambiguously show that the overall resistance, R_s+R_{ct}, of the Ti/TiN/Pd electrode is substantially lower than that of pristine TiNO, regardless of the applied overpotential, Table 1. It may then be stated that the lower performance of the Ti/TiNO/Pd electrode cannot be imputed on an increase in R_{ct}, and that other interfacial effects, probably related to the electronic structure of the surface, might be responsible (see below for discussion).

The Tafel plots are shown in Figure 6b with the indicated slopes corresponding to the low voltage range. The slope of TiNO is in the vicinity of the values usually observed for Pt-NPs which points to a Tafel-mechanism, Equation (3), controlled by the Volmer step, Equation (1) [4–6]. The

 doi:10.20944/preprints202403.1821.v1

almost double slope characterizing the Ti/TiNO/Pd-NPs rather hints to a Heyrovsky-like mechanism with the HER being primarily dependent on the rate of hydrogen desorption, Equation (2).

The chronoamperometric measurements over a period of 16h are displayed comparatively in Figure 6c. the current density of the Ti/TiNO electrode first increases (in absolute value) during the first 7 hours polarization, followed by a steady decrease with final saturation at a value of |30.5| mA/cm^2 that is slightly higher that the value at the start of the measurement. In the case of the Ti/TiN/Pd electrode, the current density first decreases in the first hour than stabilizes at a value of |27| mA/cm^2 which is roughly the value at the beginning of the measurement.

After the HER measurements, microscopic characterizations of the microstructures were performed; there were no noticeable changes to any of the samples investigated. This is well documented in Figure S2 (supplementary information) where both morphology and chemical analyses are displayed.

Table 1. the values of R_s and R_{ct} calculated using a reactive system as model.

Overvoltage (V)	R_s (Ohm)		R_{ct} (Ohm)	
	Ti/TiN	Ti/TiN/PdNPs	Ti/TiN	Ti/TiN/PdNPs
-0.4	3.36	3.45	1.121	0.52
-0.3	3.48	3.32	1.845	0.76
-0.2	3.51	3.33	5.477	1.16
-0.1	3.52	3.35	38.97	2.18

4. Discussion

4.1. HER of Oxygen Defects Containing TiN

The properties depicted above will now be discussed briefly. The surface chemistry of the TiN layer undoubtedly plays a key role in tuning the properties of this material. There is consensus that oxygen spontaneously, i.e., exothermally substitutes for nitrogen, giving rise to oxygen defects, ON, when its partial pressure exceeds 10^{-12} Torr. In the case of oxygen-rich atmospheres, the possibility of interstitial oxygen defects, Oi, formation has been also put forward using DFT [38]. In our case, where the base pressure before sputtering was 2.10^{-8} Torr, the defects that form are probably of the ON type. Because divalent oxygen is substituting trivalent N in the TiN lattice, electrical neutrality is established via the formation of Ti^{3+} vacancies, $Ti^{3+}_{(V)}$. The general stoichiometry can be expressed as $\boldsymbol{Ti^{3+}_{(1-\frac{x}{3})}Ti^{3+}_{(V)x/3}N^{3+}_{1-x}O^{2-}_{x}}$ where x may take values from 0 to 1 [30]. The impact of oxygen defects on the functional properties of TiN has been well documented and ranges from effects on its plasmonic and electronic properties to band-gap shift, depending on oxygen content [30,38]. Concerning the topic dealt with presently there has been no report detailing the effects of oxygen defects on the HER activity of TiN which stresses the novelty of the present results. Oxygen defects are thought to affect the HER properties via altering the hydrogen adsorption/desorption properties and concentration of adsorption sites, albeit a detailed investigation of the oxygen defect concentration on HER is still to be conducted. As mentioned earlier, the introduction of oxygen defects in the TiN lattice entails the formation of $Ti^{3+}_{(1-\frac{x}{3})}Ti^{3+}_{(V)x/3}N^{3+}_{1-x}O^{2-}_{x}$ which alter the electronic properties of the surrounding atoms.

Following the reasoning of Roy et al., and the schematic Figure 7 the existence of these vacancies results in the Ti^{3+}ions in the vicinity of the defect becoming more negative because they donate electrons to the electronegative N^{3-} and O^{2-} ions. A similar reasoning might be applied to those nitrogen ions adjacent to the oxygen defects. As hydrogen adsorbs both on Ti and N sites, we may expect that altering the electronic density of these sites also alters the hydrogen adsorption energy on them, possibly leading to more active sites which explains the higher performance of the TiNO layer. These assumptions are corroborated by DFT calculations described below.

Preprints.org (www.preprints.org) | NOT PEER-REVIEWED | Posted: 29 March 2024 doi:10.20944/preprints202403.1821.v1

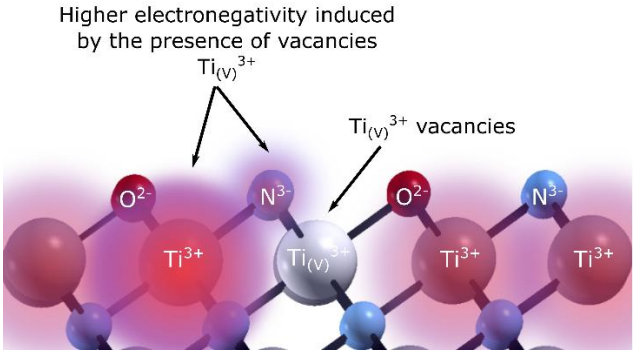

Figure 7. Schematic illustration of the electronic changes, Ti^{3+} ions in the vicinity of the defect becoming more negative. Colour coded according to the change in atomic charge, with a colour gradient from positive (red) to negative (blue).

4.2. DFT Calculations

DFT is an approach that allows the electronic structure and energetics of materials to be studied accurately. It provides insight into the distribution of electrons and calculations of the total energy of a given system. DFT has become a powerful tool for simulating the interaction between hydrogen molecules and solid surfaces [39]. When hydrogen molecules interact with TiN surfaces, several factors come into play. These include the binding energy between hydrogen and TiN, charge transfer, geometric configurations, and the effect of surface defects and impurities. DFT calculations of the adsorption energy of hydrogen on TiN and TiNO have presently allowed to test the validity of the assumptions outlined above.

Several important observations have been made regarding hydrogen adsorption on TiN surfaces. Hydrogen bonding energy represents the strength of the bond between hydrogen molecules and the surface of catalyst materials during the adsorption process. Hydrogen molecules tend to bind strongly to TiN (100) surfaces compared to TiN (111) with a difference of ~1eV, favoring the bridge sites of TiN (100) and the hole sites of TiN (111) (see Figure 8). This difference in adsorption energy weakens the ability to release hydrogen from the metal surface, increasing hydrogen poisoning and blocking active sites. Intermediate hydrogen adsorption energies play, however, a central role in hydrogen production. An optimal intermediate hydrogen adsorption energy is important for several reasons [30]. Firstly, it controls the efficiency of hydrogen evolution reactions, such as water splitting or feedstock hydrogenation, which are fundamental processes in green hydrogen production. Catalysts with the right adsorption energy can lower the activation barriers for these reactions, enabling faster and more cost- effective hydrogen production. Secondly, controlling this energy allows engineers and scientists to design catalyst materials that are selective, stable and resistant to poisoning, improving the durability of hydrogen production systems. Surface defects, such as vacancies or impurities, can enhance or prevent hydrogen adsorption, emphasizing the importance of surface quality in real world applications. To compare the results of the calculations with the experiments, oxygen impurities were introduced. The hydrogen adsorption energies were calculated at the different sites for $Ti_{1-\frac{x}{3}}N_xO_{1-x}$ (111). Due to the changes caused by the oxygen defects, a reduced adsorption energy is expected. The difference between nitrogen and oxygen in terms of electronic structure results in a redistribution of charge on the surface. This redistribution enhances hydrogen adsorption on titanium, leading to an intermediate bonding of -0.1 eV, a value which, if not in the range of the -0.04 eV known for platinum [40], is nevertheless rather promisingly low to point to $Ti_{1-\frac{x}{3}}N_xO_{1-x}$ as a very good HER catalyst. The results obtained advantageously compare to those of more sophisticated catalysts such as (Pd-O)-co-doped MoS_x [41], MoS_2 nanosheets [17],], non-metallic hybrid catalyst based on graphitic C_3N_4, and nitrogen doped graphene [18], while simultaneously affording superior opportunities with regards to scalability, easiness of preparation etc.

Preprints.org (www.preprints.org) | NOT PEER-REVIEWED | Posted: 29 March 2024 doi:10.20944/preprints202403.1821.v1

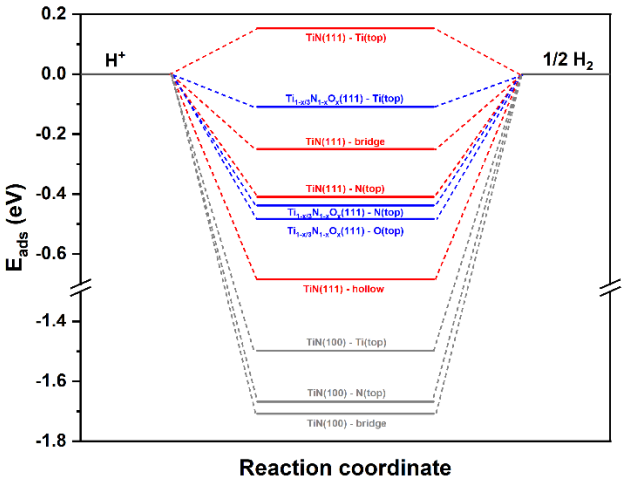

Figure 8. Hydrogen adsorption energy profile of the HER on various sites of TiN(100), TiN(111) and $Ti_{1-\frac{x}{3}}N_xO_{1-x}$ (111).

The density of states for TiN (111) (Figure 9) reveals a continuous state distribution spreading over a large range of 7.5 eV compared to TiN (100) (Figure 9), which shows a discontinuity around -1.8 eV, affecting the charge transfer from TiN to hydrogen by adsorption. Due to the few states between -1.8 eV and the Fermi level for TiN (100), more energy is required to share the electron from a deeper energy level with hydrogen, which is the opposite case for TiN (111). The overall effect of oxygen on TiN density is on Ti atoms, as changes in the local environment around Ti atoms due to oxygen defects affect its catalytic activity. A closer look at Ti shows that the oxygen defects cause changes in the density of states in Ti (Figure 10); Ti4d and Ti3p are very well distributed across the energy axis. The "good" hydrogen adsorption energy is reflected in the positioning of the density of states at around -5 eV and -13 eV. TiN is a well-known refractory material with a high density of electrons in the conduction band due to the presence of nitrogen. When oxygen defects are introduced, they can act as electron acceptors, leading to the formation of titanium vacancies, mentioned above, and a shift in the electronic structure of titanium. This results in the creation of localized energy states within the band. The presence of oxygen-related states leads to changes in the electronic band structure. This change can affect the electrical conductivity of the material and its ability to participate in charge transfer processes [42].

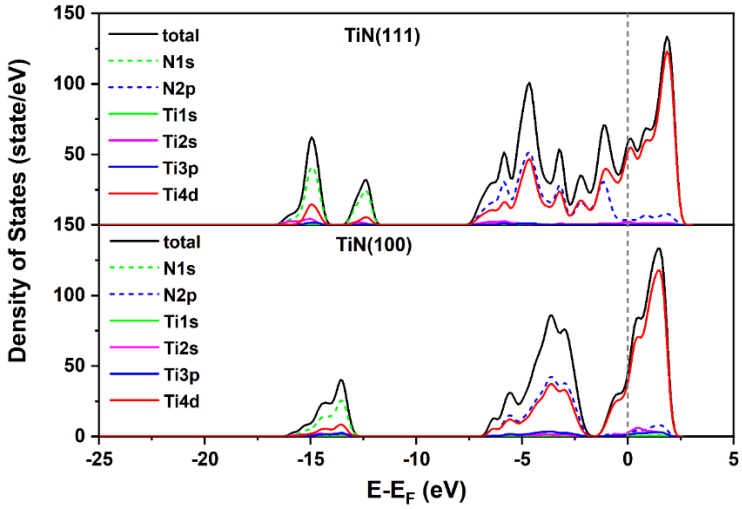

Figure 9. Orbital electronic density of states for TiN(111) and TiN(100). E_F denotes the Fermi level.

 doi:10.20944/preprints202403.1821.v1

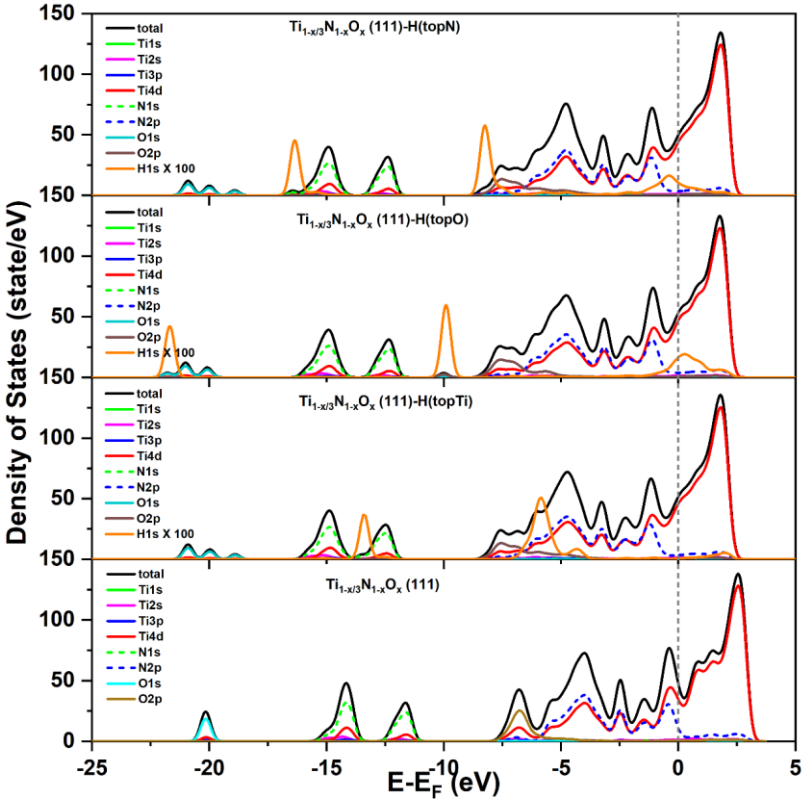

Figure 10. Orbital electronic density of states for $Ti_{1-\frac{x}{3}}N_xO_{1-x}$ (111), and Hydrogen atoms adsorbed on different sites Ti, N, and O. H density of states are magnified by 100 for comparison. E_F denotes the Fermi level.

In summary, the presence of oxygen impurities in TiN surfaces alters the adsorption of hydrogen on titanium by changing the electronic structure of titanium. The introduction of oxygen-related electronic states leads to changes in the charge distribution and electronic structure, which in turn affects the interaction between hydrogen molecules and the TiN surface. This has implications for various applications where hydrogen adsorption on TiN surfaces is important, including catalysis and hydrogen storage. Thus, strategies to introduce oxygen defects at certain levels can improve the catalytic performance of TiN.

4.3. Pd-Top-Layer Effects

The question which now arises is as to why Pd-NPs depress the performance of the whole structure, although Pd is known to be a potent HER catalyst. As shown in Figure 5a, sputtering a thin layer of Pd on TiN results in a marked decrease of the overall performance, despite the Rct values recorded were lower than those of TiNO. Two possible explanations having the same outcome may be suggested. The first invokes in the scavenging of the surface oxygen defects by the Pd-atoms, leading to the formation of PdO and possibly annihilation of $Ti_{(V)}^{3+}$. This has been indeed observed via scanning tunneling microscopy on Pd-NPs that were deposited on non-stoichiometric TiO_2 (that contains $Ti_{(V)}^{3+}$) [42]. A second possibility invokes the formation of an ultrathin TiO_x layer on the Pd-NPs [43]. Whether the first or second case applies is subject to speculation until a proper analytical method is used to discriminate between them. The outcome is however the same as the electronic and defect structure of TiNO will be altered in both cases, leading to changes in the electrocatalytic performance.

 doi:10.20944/preprints202403.1821.v1

5. Conclusions

In conclusion, TiN and TiN-PdNPs were processed on Ti-substrates via physical vapor deposition. Morphological characterization shows a nanostructured, highly porous surfaces with spiky nano-crystallites. XRD investigations reveal a non-stoichiometric rock salt TiN structure, with eventually Pd-NPs. The surface chemistry studied by X-ray photoelectron spectroscopy unambiguously shows the existence of oxygen defects pointing to the formation of a TiNO phase at the surface. The suitability of the TiNO and TiNO/Pd-NPs structures as electrocatalysts for the hydrogen evolution reaction was evaluated via linear sweep voltammetry, Tafel plots and electrochemical impedance spectroscopy. TiNO shows an outstanding performance towards HER, and DFT calculations reveal that oxygen impurities in TiN surfaces have a significant influence on hydrogen adsorption energy through their effect on the electronic structure of titanium. The introduction of oxygen-related electronic states changes the charge distribution and electronic structure, affecting the interaction of hydrogen molecules with the TiNO surface. This has important implications for applications such as catalysis and hydrogen storage, where hydrogen adsorption on TiN is critical. Introducing oxygen defects at controlled levels can improve the catalytic behaviour of TiN. When a thin Pd-layer is sputtered on TiNO a drastic performance decrease is observed; this is thought to arise from the scavenging of oxygen defects by Pd atoms, entailing the formation of PdO or an ultrathin TiOx layer on the Pd-NPs, possibly removing Ti^{3+} vacancies. This is a further proof of the importance of TiNO surfaces for the HER performance. Thus, ensuing studies will have to quantify the effects of oxygen defects in TiN on HER by controlling their concentration. This may pave the way for a high-performance catalyst that is at the same time cheap, robust and easily scalable.

Supplementary Materials: The following supporting information can be downloaded at: Preprints.org, Figure S1: a photograph of a large area thin film; Figure S2: morphology of the films after the HER experiments

Author Contributions: Conceptualization ME; investigation AL; theoretical modelling AL; data curation ME; writing AL, ME; final editing ME..

Funding: Ayoub Laghrissi was funded by the INTERREG VA Project “CheckNano”, project # 086- 1.1 – 17.

Acknowledgments: Thanks are due to Franz Faupel, Technical Faculty, CAU, Kiel, for permission to use the XPS Facility and to Thomas Strunskuss for assistance with the measurements

Conflicts of Interest: The authors declare no conflicts of interest.

References

1. Hohmeyer, O.H.; Bohm, S. Trends toward 100% renewable electricity supply in Germany and Europe: a paradigm shift in energy policies. WIREs Energy Environ. 2015, 4, 74-97.
2. Dincer, I.; Acar, C. Innovation in hydrogen production. Int. J. Hydrog. Energy 2017, 42, 14843-14864.
3. Fastmarkets. 2020.
4. Conway, B.E.; Tilak, B.V. Interfacial processes involving electrocatalytic evolution and oxidation of H2, and the role of chemisorbed H. Electrochimica Acta 2002, 47, 3571-3594.
5. Bockris, J.O.; Conway, B.E. Butterworths Sci Publ. 1954.
6. Eley, D.D.; Pines, H.; Weisz, P.B. Acad. Press Inc. 1992.
7. Bhardwaj, M.; Balasubramaniam, R. Uncoupled non-linear equations method for determining kinetic parameters in case of hydrogen evolution reaction following Volmer–Heyrovsky–Tafel mechanism and Volmer–Heyrovsky mechanism. Int. J. Hydrog. Energy 2008, 33, 2178-2188.
8. Shinagawa, T.; Garcia-Esparza, A.T.; Takanabe, K. Insight on Tafel slopes from a microkinetic analysis of aqueous electrocatalysis for energy conversion. Sci. Rep. 2015, 5, 13801.
9. Eftikhari, A. Electrocatalysts for hydrogen evolution reaction. Int. J. Hydrog. Energy 2017, 42, 11053-11077.
10. Stratton, S.M.; Zhang, S.; Montemore, M.M. Addressing complexity in catalyst design: From volcanos and scaling to more sophisticated design strategies. Surf. Sci. Rep. 2023, 78, 100597.
11. Laghrissi, A.; Es-Souni, M. Au-Nanorods Supporting Pd and Pt Nanocatalysts for the Hydrogen Evolution Reaction: Pd Is Revealed to Be a Better Catalyst than Pt. Nanomaterials 2023, 13, 2007.
12. Zhang, N.; Shao, Q.; Xiao, X.; Huang, X. Advanced Catalysts Derived from Composition-Segregated Platinum–Nickel Nanostructures: New Opportunities and Challenges. Adv. Funct. Mater. 2019, 29, 1808161.

13. Hu, D.; Fan, W.; Liu, Z.; Li, L. Three-Dimensionally Hierarchical Pt/C Nanocomposite with Ultra-High Dispersion of Pt Nanoparticles as a Highly Efficient Catalyst for Chemoselective Cinnamaldehyde Hydrogenation. ChemCatChem 2018, 10, 779.
14. Sanyal, U.; Song, Y.; Singh, N.; Fulton, J.L.; Herranz, J.; Jentys, A.; Gutiérrez, O.Y.; Lercher, J.A. Structure Sensitivity in Hydrogenation Reactions on Pt/C in Aqueous-phase. ChemCatChem 2019, 11, 575.
15. Ostovari Moghaddam, A.; Trofimov, E.A. Toward expanding the realm of high entropy materials to platinum group metals: A review. J. Alloys Compd. 2021, 851, 156838.
16. McKone, J.R.; Warren, E.L.; Bierman, M.J.; Boettcher, S.W.; Brunschwig, B.S.; Lewis, N.S.; Gray, H.B. Evaluation of Pt, Ni, and Ni–Mo electrocatalysts for hydrogen evolution on crystalline Si electrodes Energy Environ. Sci. 2011, 4, 3573-3583.
17. Voiry, D.; Salehi, M.; Silva, R.; Fujita, T.; Chen, M.; Asefa, T.; Shenoy, V.B.; Eda, G.; Chhowalla, M. Conducting MoS2 Nanosheets as Catalysts for Hydrogen Evolution Reaction. Nano Lett. 2013, 13, 6222-6227.
18. Zheng, Y.; Jiao, Y.; Zhu, Y.; Li, L.H.; Han, Y.; Chen, Y.; Du, A.; Jaroniec, M.; Qiao, S.Z. Hydrogen evolution by a metal-free electrocatalyst. Nat. Commun. 2014, 5, 3783.
19. Laghrissi, A.; Es-Souni, M. A TiN@Au-NR Plasmonic Structure with Tunable Surface Plasmon Resonance Depending on TiN to Au Thickness Ratio. Plasmonics 2021, 16, 49–57.
20. Santecchia, E.; Hamouda, A.M.S.; Musharavati, F.; Zalnezhad, E.; Cabibbo, M.; Spigarelli, S. Wear resistance investigation of titanium nitride-based coatings. Ceram. Int. 2015, 41, 10349-10379.
21. Zhang, J.; Hu, H.; Liu, X.; Li, D.-S. Development of the applications of titanium nitride in fuel cells. Mater. Today Chem. 2019, 11, 42-59.
22. van Hove, R.P.; Sierevelt, I.N.; van Royen, B.J.; Nolte, P.A. Titanium-Nitride Coating of Orthopaedic Implants: A Review of the Literature. BioMed Res. Int. 2015, 2015, 485975.
23. Ahangarani, S.; Sabour Rouhaghadam, A.; Azadi, M. A Review on Titanium Nitride and Titanium Carbide Single and Multilayer Coatings Deposited by Plasma Assisted Chemical Vapor Deposition. Int. J. Eng. 2016, 29, 677-687.
24. Liu, L.M.; Wang, S.Q.; Ye, H.Q. First-principles study of the effect of hydrogen on the metal–ceramic interface. J. Phys.: Condens. Matter 2005, 17, 5335-5348.
25. Siodmiak, M.; Govind, N.; Andzelm, J.; Tanpipat, N.; Frenking, G.; Korkin, A. Theoretical Study of Hydrogen Adsorption and Diffusion on TiN(100) Surface. Phys. Status Solidi B 2001, 226, 29-36.
26. Giannozzi, P.; Baroni, S.; Bonini, N.; Calandra, M.; Car, R.; Cavazzoni, C.; Ceresoli, D.; Chiarotti, G.L.; Cococcioni, M.; Dabo, I. QUANTUM ESPRESSO: a modular and open-source software project for quantum simulations of materials. J. Phys.: Condens. Matter 2009, 21, 395502.
27. Giannozzi, P.; Andreussi, O.; Brumme, T.; Bunau, O.; Nardelli, M. B.; Calandra, M.; Car, R.; Cavazzoni, C.; Ceresoli, D.; Cococcioni, M. Advanced capabilities for materials modelling with Quantum ESPRESSO. J. Phys.: Condens. Matter 2017, 29, 465901.
28. Giannozzi, P.; Baseggio, O.; Bonfà, P.; Brunato, D.; Car, R.; Carnimeo, I.; Cavazzoni, C.; de Gironcoli, S.; Delugas, P.; Ruffino, F. F.; Ferretti, A.; Marzari, N.; Timrov, I.; Urru, A.; Baroni, S.. Quantum ESPRESSO toward the exascale. J. Chem. Phys. 2020, 152, 154105.
29. Perdew, J.P.; Burke, K.; Ernzerhof, M. Generalized Gradient Approximation Made Simple. Phys. Rev. Lett. 1996, 77, 3865.
30. Roy, M.; Sarkar, K.; Som, J.; Pfeifer, M. A.; Craciun, V.; Schall, J.D.; Aravamudhan, S.; Wise, F.W.; Kumar, D. Modulation of Structural, Electronic, and Optical Properties of Titanium Nitride Thin Films by Regulated In Situ Oxidation. ACS Appl. Mater. Interfaces 2023, 15, 4733−4742.
31. Ahmed, M.; Xinxin, G. A review of metal oxynitrides for photocatalysis. Inorg. Chem. Front. 2016, 3, 578−590.
32. Graciani, J.; Hamad, S.; Sanz, J.F. Changing the physical and chemical properties of titanium oxynitrides
33. TiN1−xOx by changing the composition. Phys. Rev. B 2009, 80, 184112.
34. Venkataraj, S.; Severin, D; Mohamed, S.H.; Ngaruiya, J.; Kappertz, O.; Wuttig, M. Towards understanding the superior properties of transition metal oxynitrides prepared by reactive DC magnetron sputtering. Thin Solid Films 2006, 502, 228−234.
35. Amin, M.A.; Fadlallah, S.A.; Alosaimi, G.S. In situ aqueous synthesis of silver nanoparticles supported on titanium as active electrocatalyst for the hydrogen evolution reaction. Int. J. Hydrog. Energy 2014, 39, 19519-19540
36. Durst, J. Siebel, A.; Simon, C.; Hasché, F.; Herranz, J. and Gasteiger, H. A. New insights into the electrochemical hydrogen oxidation and evolution reaction mechanism. Energy Environ. Sci. 2014, 7, 2255–2260.
37. Han, Y. Xin Yue, X.; Jin, Y.; Huang, X. and Shen, P. K. Hydrogen evolution reaction in acidic media on single-crystalline titanium nitride nanowires as an efficient non-noble metal electrocatalyst. J. Mater. Chem. A 2016, 4, 3673-3677.
38. El-Khodary, S.A.; Cui, Y.; Bu, Y.; Lian, J. Electrochem. Capacitors. 2023, 1, 1-60.

 doi:10.20944/preprints202403.1821.v1

39. Kumar, R. Nayak, S.;Garbrecht, M.; Bhatia, V.; Pillai, A. I. K. ; Gupta, M.;Shivaprasad, S. M.; Saha, B. Clustering of oxygen point defects in transition metal nitrides. J. Appl. Phys. 2021, 129, 055305.
40. Guo, Y. Zhang, C.; Wu, Y.; Yu, H.; Zhang, S.; Du, A; Ostrikov, K. K.; Zheng, J. and Li, X. Direct conversion of metal organic frameworks into ultrafine phosphide nanocomposites in multicomponent plasma for wide pH hydrogen evolution. J. Mater. Chem. A 2020, 8, 10402.
41. Exner, K.S. On the optimum binding energy for the hydrogen evolution reaction: How do experiments contribute?. Electrochem. Sci. Adv. 2022, 2, e2100101.
42. Zhan, Y. Zhou, X.; Nie, H.; Xu, X.; Zheng, X.; Hou, J.; Duan, H.; Huang, S. and Yang, Z. Designing Pd/O co-doped MoSx for boosting the hydrogen evolution reaction J. Mater. Chem. A 2019, 7, 15599.
43. Bennett, R.A.; Stone, P.; Bowker, M. Pd nanoparticle enhanced re-oxidation of non-stoichiometric TiO2: STM imaging of spillover and a new form of SMSI. Catal. Lett. 1999, 59, 99–105.
44. Chenakin, S.P.; Melaet, G.; Szukiewicz, R.; Kruse, N. XPS study of the surface chemical state of a Pd/(SiO2 + TiO2) catalyst after methane oxidation and SO2 treatment. J. Catal. 2014, 312, 1–11.